Geometrodynamic approach to conjugate points and the Maslov index

A. Vergel [1,2,*] J. Montes [1,2,3,†] and F. Borondo [1,3,‡]

[1]*Instituto de Ciencias Matemáticas (ICMAT), Cantoblanco, 28049 Madrid, Spain*

[2]*Grupo de Sistemas Complejos, Universidad Politécnica de Madrid, 28040 Madrid, Spain*

[3]*Departamento de Química, Universidad Autónoma de Madrid, Cantoblanco, 28049 Madrid, Spain*

(Received 8 July 2022; accepted 1 December 2022; published 28 December 2022)

Maslov indices are an essential ingredient in the semiclassical approaches to quantum mechanics, as they are also related to the conjugate points of the corresponding trajectory, which reflects the dynamics in its neighborhood. In this paper, we show how these important topological parameters can be computed using the geometrodynamic approach to dynamics. Illustrations in two- and three-dimensional systems are presented and discussed.

DOI: 10.1103/PhysRevE.106.064213

I. INTRODUCTION

The first attempt to introduce energy quantization in physical systems in order to explain atomic spectra was carried out by Bohr [1] in the Kepler model for the hydrogen atom. He (semiclassically) quantized the one-dimensional action, which is related to the energy, with Planck's constant as $\int p\, dq = 2\pi\hbar n$ wih $n = 1, 2, \ldots$. Despite the simplicity of this approach, it was successful for a number of reasons, the main one being that the model was separable. The theory was extended by Sommerfeld [2] and Epstein [3], and it has been known ever since as the Bohr-Sommerfeld (BS) quantization rule. Later work by Einstein [4] and Ehrenfest [5] emphasized the relevance of adiabatic invariants for this task, and it was the former that in 1917 clarified the issue [6], stating that, for integrable systems, it is the total action $S(E) = \int p_i dq^i$ (Einstein summation rule on repeated indices is used here and throughout the paper) the proper magnitude to quantize and moreover that this should be done along the N (dimensionality of the system) topological independent circuits $\mathcal{C}_k$ defining the associated dynamical torus [7] of energy E,

$$S(E) = \oint_{\mathcal{C}_k} p_i dq^i = 2\pi\hbar\left(n_k + \frac{\mu_k}{4}\right),$$
$$k = 1, 2, \ldots, N, \quad n_k = 0, 1, 2, \ldots. \tag{1}$$

The original Einstein's formulation lacked the topological term μ_k, which was later introduced by Maslov [8], Brillouin [9], and Keller [10]. It is important to note that μ_k are topological invariants, and their values do not depend on the coordinates or parametrizations. Equation (1), which. puts Bohr theory on firm ground, is known as the Einstein-Brillouin-Keller (EBK) quantization rule. Furthermore, both the action and Maslov indices appear not only in this expression but also in the associated (semiclassical) wave functions [11].

These results are related to the eikonal equation: $(d/ds)[n(d\mathbf{q}/ds)] = \nabla n$ [12] of geometric optics [13] in the limit $\hbar \to 0$ when defining the refractive index as $n(\mathbf{q}) = \{2[E - V(\mathbf{q})]\}^{1/2}$, where s is the corresponding arc-length. Both in this approximation and in the Hamilton-Jacobi the generating function equals the classical action divided by $\hbar$. This relates Fermat and Mapertuis principles.

Maslov indices are also related to catastrophe theory [14,15], a branch of bifurcation theory, which is also a particular special case of more general singularity theory in geometry, especially in connection with caustics, and the accumulation of rays along them that takes place in optics [13].

The BS condition (including the proper action, mechanical and topological) can be applied to periodic orbits to calculate, for example, scarred functions [16–18], which are highly localized quantum wave functions playing a fundamental role in quantum chaos theory [19].

It is also interesting to remark here that Einstein knew very well Poincaré's work on the three-body problem, and then he remarked in the last four lines of his 1917 paper [6] that the existence of invariant tori was not always the case in the dynamic of generic Hamiltonian system, this precluding the use of Eq. (1) and making his theory far from complete. Actually, it was not until the 1970s that Gutzwiller published his celebrated trace formula [20], able to semiclassically quantize all kind of systems, regardless if the dynamics was regular or chaotic. In his derivation, the author started from a semiclassical approximation to the quantum propagator for long times in order to include the extra phases at the conjugate points, obtained by stationary phase approximation of the Feynman path integrals, followed by Laplace transformation to obtain the corresponding Green function and finally took the trace [20]. Gutzwiller's trace formula is expressed solely in terms of all periodic orbits of the system. Again, here actions and Maslov indices play a crucial role in the theory.

It should be remarked that although semiclassical theories [16] seem to have been made obsolete by quantum mechanics,

*alberto.vergel.otero@upm.es
†jmontes3@alumni.unav.es
‡f.borondo@uam.es

this is not the case, since they still play a fundamental role in the understanding of many processes in atomic and molecular physics, this including quantum chaos [19], which is important for entanglement, decoherence, and quantum computing [21].

Very general methods to compute Maslov indices have been described in the literature [22–24]. They typically require us to calculate the number of full semiturns performed in phase space by the invariant manifolds associated to the orbit along one period. These manifolds can be studied by following the evolution of the monodromy matrix eigenvectors associated to the motion [17,18], and this can be done choosing different coordinate systems [22].

In this paper, we present an original way to compute Maslov indices for a given orbit based on the geometrodynamic formalism, which is a way to describe dynamics in purely geometrical terms. As such, it is tightly connected to the theory of relativity, although in this work we will restrict ourselves to classical mechanics. For this purpose a tensor metric is defined in a Riemannian manifold, whose structure determines the way to measure lengths, angles, and areas in the tangent space [25,26]. This tensor is a dynamical magnitude that evolves, for example, with time or, as in this work, with energy, contrary to what happens in Newton's theory, which is defined with a Euclidean tensor metric where geometry is static.

In two related studies [27,28], a general formula for computing the Maslov index for geodesics in locally symmetric semi-Riemannian manifold is studied. In some special cases for invariant metrics on a Lie group this calculation can be performed by counting the number of conjugate points (with their multiplicity) along a distinguished geodesic. In this line, our work considers the case of a general Riemannian manifold.

The geometrodynamic formalism has successfully been used in the literature to study nonlinear Hamiltonian systems using different metrics, such as those of Eisenhart [29], Finsler [30–33], Jacobi [34], and others [35,36]. In this way the stability, transitions to chaos, Lyapunov exponent, and other topological dynamical aspects have been studied in systems ranging from low dimension to the thermodynamic limit [37–43]. In particular, studies about the transition from classical order to chaos [44,45], and others comparing classical and quantum phase structures, or the quantum manifestations of chaos in the vibrational dynamics of molecular systems, have been published in our group [46–51]. Moreover, different chaos indicators have been successfully defined using this method by us [52,53] and others [54].

The geometrodynamical formalism will be applied in this work to study the focusing of neighboring trajectories with respect to a reference (usually unstable) orbit using the Jacobi-Levi-Civita (JLC) equation as a way to compute the corresponding Maslov indices, and different examples in two- and three-dimensional systems will be presented as illustrations.

The organization of the paper is as follows. First, we present in Sec. II the theoretical aspects of our work, organized in three subsections: In the first one (Sec. II A) we describe the geometrodynamic frame and the corresponding Jacobi equation for geodesic flux to make our paper self-contained. Next, we present in Sec. II B the Jacobi-Levi-Civita equation in two and three dimensions and discuss in Sec. II C how it can be applied to the localization of the conjugate points and calculation of Maslov indices of a periodic orbit. Finally, we present as an illustration some results in Sec. III for two- and three-dimensional examples with regular and chaotic dynamics.

II. THEORY

A. Maupertuis principle and the Jacobi metric

In this subsection, we recast the dynamical system theory into a geometric formalism in which forces are made to cancel, and therefore motions are free, although constrained into a Riemannian manifold called *mechanical manifold (MM)*.

Classical mechanics can be formally derived from the Maupertuis principle if a Lagrangian function is previously defined in terms of generalized coordinates $\mathbf{q}$ and their velocities $\dot{q}^i = dq^i/dt$ as

$$L(\mathbf{q}, \dot{\mathbf{q}}, t) = T\left(q^i, \frac{dq^i}{dt}\right) - V(\mathbf{q}) = \frac{1}{2} a_{ij}(\mathbf{q}) \frac{dq^i}{dt} \frac{dq^j}{dt} - V(\mathbf{q}), \tag{2}$$

where T and V are the kinetic and potential functions, respectively, and a_{ij} is the mass matrix. Associating a covariant vector of conjugate momenta $\mathbf{p}$ with the Lagrangian L,

$$p_i \longleftrightarrow a_{il} \frac{dq^l}{dt} = \frac{\partial L(\mathbf{q}, \dot{\mathbf{q}}, t)}{\partial \dot{q}^i}, \tag{3}$$

Maupertuis principle establishes that natural motions take place only along those trajectories, γ, making stationary the action integral,

$$\mathcal{A} = \int_{\gamma(t)} p_i \, dq^i = \int_{\gamma(t)} \frac{\partial L}{\partial \dot{q}^i} \dot{q}^i \, dt = \int_{\gamma(t)} 2T \, dt, \tag{4}$$

where T is assumed to depend quadratically on $\mathbf{p}$. For conservative systems $E = T + V$, this principle is expressed as

$$\delta \mathcal{A} = \delta \int_{\gamma(t)} \sqrt{2[E - V(\mathbf{q})] \, a_{ij}(\mathbf{q}) \, \dot{q}^i \dot{q}^j} \, dt = 0. \tag{5}$$

Now, defining (M, g_J) as the MM with $\mathbf{q} = (q^1, q^2, \ldots, q^N) \in M$ and E = constant energy, with the metric g_J, called the *Jacobi metric*, expressed in coordinates as

$$g_J = g_{ij}(\mathbf{q}) = 2[E - V(\mathbf{q})] \, a_{ij}(\mathbf{q}), \tag{6}$$

the trajectories fulfilling the previous principle are the geodesic lines for this metric, i.e.,

$$\delta \mathcal{A} = \delta \int_{\gamma(s)} ds = 0, \tag{7}$$

where s is the arc-length given by

$$ds = 2[E - V(\mathbf{q})] \, dt. \tag{8}$$

In this setup, natural motions are interpreted as geodesic lines in MM, and the dynamical magnitudes can be associated with geometric ones. In Table I, we present the equivalence among some relevant such dynamical and geometrodynamic magnitudes in classical mechanics.

TABLE I. Equivalence among some relevant magnitudes in dynamics and geometrodynamics in classical mechanics.

Dynamics	Geometrodynamics
Time, t	Arc length, s
Potential, V	Metric, g_{ij}
Force, $-\partial V$	Christoffel symbols, $-\Gamma^i_{jk}$
Trajectories	Geodesics
Conserved quantities	Symmetries
Stability	Curvature

Furthermore, the geodesic lines fulfill the relation $\nabla_{\dot\gamma}\dot\gamma = 0$ (where ∇ is the Riemannian connection for g_{ij}), which in terms of local coordinates is written as

$$\nabla_{\dot\gamma}\dot\gamma = \frac{d^2q^i}{ds^2} + \Gamma^i_{jk}\frac{dq^j}{ds}\frac{dq^k}{ds} = 0, \tag{9}$$

where Γ^i_{jk} are the so-called Christoffel symbols for the metric g_{ij} and s the arc-length parameter. Changing to parameter t, i.e., $\dot q^i = dq^i/dt$, Eq. (9) transforms into

$$\ddot q^i + \tilde\Gamma^i_{jk}\dot q^j\dot q^k = -\partial_l V a^{il}, \tag{10}$$

the *Euler-Lagrange* equations, where $\tilde\Gamma^i_{jk}$ are the so-called Christoffel symbols for the metric $a_{ij}(\mathbf{q})$, and then trajectories under the potential $V(\mathbf{q})$ in the coordinates space with metric $a_{ij}(\mathbf{q})$ are transformed into geodesic lines in MM.

Let us remark that the integral in the left-hand side of the EBK quantization rule (1) equals the expression for the action $\mathcal{A}$ in the Maupertuis principle (4). This indicates that action is relevant in both classical and quantum theory [55]. Moreover, the quantization for the total action S along a periodic orbit is equivalent to quantize its length with the Jacobi metric (6).

B. Jacobi-Levi-Civita equation

Let us now consider the laws governing the dispersion of geodesic lines which are close to a reference one. This spreading is directly related with the curvature of the MM, and it has been used by us in the past to define new descriptors for chaotic behavior in Hamiltonian systems [52,53].

The sectional curvature $R(P,\sigma)$ at point $P \in M$, where $\sigma \subset T_PM$ is the tangent plane to the Riemannian manifold M at this point, determines the geodesic dispersion at P, initially tangent to M. In the two-dimensional case, R corresponds to the Gaussian curvature. We introduce now the Riemann-Christoffel curvature tensor $R(\mathbf{X},\mathbf{Y}) : T_PM \longrightarrow T_PM$, defined as

$$R(\mathbf{X},\mathbf{Y})\mathbf{Z} = \nabla_{\mathbf{Y}}\nabla_{\mathbf{X}}\mathbf{Z} - \nabla_{\mathbf{X}}\nabla_{\mathbf{Y}}\mathbf{Z} + \nabla_{[\mathbf{X},\mathbf{Y}]}\mathbf{Z}, \tag{11}$$

with $\mathbf{X},\mathbf{Y},\mathbf{Z} \in T_PM$, and ∇ the Riemannian connection for g_{ij}. This curvature tensor can be written in a local chart with a canonical basis $\{\mathbf{e}_i\}$ (see schematic diagram in Fig. 1), as

$$R(\mathbf{e}_k,\mathbf{e}_l)\mathbf{e}_m = R^i_{klm}\mathbf{e}_i, \text{ with}$$
$$R^i_{klm} = \frac{\partial\Gamma^i_{km}}{\partial x^l} - \frac{\partial\Gamma^i_{kl}}{\partial x^m} + \Gamma^i_{ls}\Gamma^s_{km} - \Gamma^i_{ms}\Gamma^s_{kl}, \tag{12}$$

where Γ^i_{km} is the Christoffel symbols for the metric g_{ij}. The evolution of the dispersion of the geodesic flow, $\mathbf{J}(s)$, along

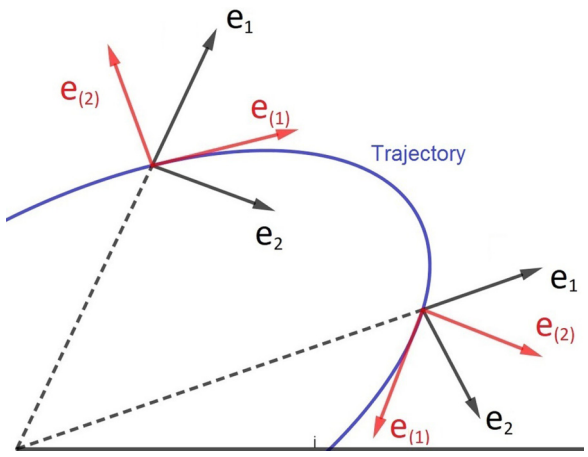

FIG. 1. Canonical basis $\{\mathbf{e}_1,\mathbf{e}_2\}$ (black) in polar coordinates and parallelly transported comoving basis $\{\mathbf{e}_{(1)},\mathbf{e}_{(2)}\}$ (red) at two different points along a geodesic (blue). See the text for details.

a reference geodesic line $\gamma(s)$ in M, $\gamma : s \in [0,a] \to M$ (see schematic diagram in Fig. 2), is governed by the JLC equation (also known as the *Jacobi* equation),

$$\frac{D^2\mathbf{J}}{ds^2} + R[\dot\gamma(s),\mathbf{J}(s)]\,\dot\gamma(s) = \mathbf{0}, \tag{13}$$

where D/ds is the covariant derivative relative to the Riemannian manifold MM, $\dot\gamma(s) = d\mathbf{q}/ds$, and ds is the arc-length differential. In local coordinates this expression reads

$$\frac{D^2J^i}{ds^2} = -R^i_{jkl}\dot\gamma^j\dot\gamma^l J^k = -\mathbb{S}^i_j J^j, \tag{14}$$

where $\mathbb{S}^i_j$ is the *stability tensor*.

Finally, expression (14) can be conveniently written in terms of a comoving frame $\{\mathbf{e}^i_{(\alpha)}\}$, which is assumed orthonormal, i.e., $g_{ij}(\mathbf{q})\,\mathbf{e}^i_{(a)}\mathbf{e}^j_{(b)} = \delta_{ab}$, moving parallel along the reference geodesic line $\gamma(s)$ (as shown schematically for the two-dimensional case in Fig. 1). This comoving basis can be expressed in terms of the canonical basis derived from the local chart as

$$\mathbf{e}_{(i)} = \mathbf{e}^j_{(i)}\mathbf{e}_j, \qquad i = 1,2,\ldots,N, \tag{15}$$

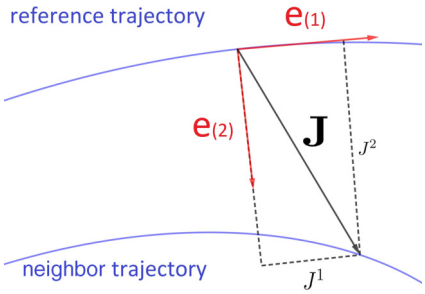

FIG. 2. Evolution of $\mathbf{J}$ along the reference geodesic, projected over the parallely transported comoving basis $\{\mathbf{e}_{(1)},\mathbf{e}_{(1)}\}$. See the text for details.

where $D\mathbf{e}_{(i)}/ds = 0$ (parallelly transported) is given in local coordinates by

$$\left[\frac{d\mathbf{e}^{\alpha}_{(i)}}{dt} + \mathbf{e}^{\mu}_{(i)}\Gamma^{\alpha}_{\mu\beta}\frac{dq^{\beta}}{dt}\right]\mathbf{e}_{\alpha} = 0. \tag{16}$$

Let us remark that the local evolution of the $\mathbf{e}^{\alpha}_{(i)}$ components of the new comoving basis can be approximated by Taylor expansion as

$$\mathbf{e}^{\alpha}_{(i)}|_t = \mathbf{e}^{\alpha}_{(i)}|_{t_0} - \mathbf{e}^{\mu}_{(i)}\Gamma^{\alpha}_{\mu\beta}\frac{dq^{\beta}}{dt}\bigg|_{t_0}(t-t_0) + \mathcal{O}(t-t_0)^2, \tag{17}$$

taking the vector tangent to the reference geodesic line $\mathbf{e}_{(1)}(s) = \dot{\gamma}(s)$ as the first one in the comoving basis.

Let us next derive specific expressions for the two- and three-dimensional cases.

1. The JLC equation for the two-dimensional case

For the two-dimensional case, $N = 2$, the new comoving basis in terms of the canonical one reads

$$\begin{aligned}\mathbf{e}_{(1)}(s) &= \dot{\gamma}^1(s)\,\mathbf{e}_1(s) + \dot{\gamma}^2(s)\,\mathbf{e}_2(s),\\ \mathbf{e}_{(2)}(s) &= \sqrt{a_{22}/a_{11}}\dot{\gamma}^2\,\mathbf{e}_1(s) - \sqrt{a_{11}/a_{22}}\dot{\gamma}^1\,\mathbf{e}_2(s).\end{aligned} \tag{18}$$

In this comoving frame $\{\mathbf{e}_{(1)}, \mathbf{e}_{(2)}\}$, $\mathbf{J}(s)$ is expressed as $\mathbf{J}(s) = J^i(s)\mathbf{e}_{(i)}(s)$, $i = 1, 2$, as shown in Fig. 2, and therefore the JLC equation (13) with $\mathbf{v} = \dot{\gamma}$ reads

$$\begin{pmatrix}\dfrac{d^2J^1}{ds^2}\\ \dfrac{d^2J^2}{ds^2}\end{pmatrix} + \begin{bmatrix}\langle R(\mathbf{v},\mathbf{e}_{(1)})\mathbf{v},\mathbf{e}_{(1)}\rangle & \langle R(\mathbf{v},\mathbf{e}_{(2)})\mathbf{v},\mathbf{e}_{(1)}\rangle\\ \langle R(\mathbf{v},\mathbf{e}_{(1)})\mathbf{v},\mathbf{e}_{(2)}\rangle & \langle R(\mathbf{v},\mathbf{e}_{(2)})\mathbf{v},\mathbf{e}_{(2)}\rangle\end{bmatrix}\begin{pmatrix}J^1\\ J^2\end{pmatrix} = 0, \tag{19}$$

where $\langle,\rangle$ is the scalar product and $\langle\mathbf{e}_i,\mathbf{e}_j\rangle = g_{ij}$ the metric coefficients. If $\mathbf{v} = \mathbf{e}_{(1)} = \dot{\gamma}$ and considering the symmetries of the curvature tensor, i.e., $\langle R(\mathbf{e}_i,\mathbf{e}_j)\mathbf{e}_k,\mathbf{e}_l\rangle = R_{ijkl} = R_{klij} = -R_{jikl} = -R_{ijlk}$, then Eq. (19) can be diagonalized, obtaining

$$\begin{pmatrix}\dfrac{d^2J^1}{ds^2}\\ \dfrac{d^2J^2}{ds^2}\end{pmatrix} + \begin{bmatrix}0 & 0\\ 0 & \langle R(\mathbf{e}_{(1)},\mathbf{e}_{(2)})\mathbf{e}_{(1)},\mathbf{e}_{(2)}\rangle\end{bmatrix}\begin{pmatrix}J^1\\ J^2\end{pmatrix} = 0, \tag{20}$$

where the comoving basis representing the stability tensor eigenvectors differ from the N-dimensional general case. Now, by considering the relation

$$|\mathbf{e}_{(1)}\wedge\mathbf{e}_{(2)}| = \sqrt{|\mathbf{e}_{(2)}||\mathbf{e}_{(2)}| - \langle\mathbf{e}_{(1)},\mathbf{e}_{(2)}\rangle} = 1, \tag{21}$$

where $\wedge$ represents the dot product, we have

$$\begin{aligned}\langle R(\mathbf{e}_{(1)},\mathbf{e}_{(2)})\mathbf{e}_{(1)},\mathbf{e}_{(2)}\rangle &= \frac{\langle R(\mathbf{e}_{(1)},\mathbf{e}_{(2)})\mathbf{e}_{(1)},\mathbf{e}_{(2)}\rangle}{|\mathbf{e}_{(1)}\wedge\mathbf{e}_{(2)}|^2}\\ &= K(\mathbf{e}_{(1)},\mathbf{e}_{(2)}) \equiv K(\sigma),\end{aligned} \tag{22}$$

where $K(\sigma)$ is the sectional curvature corresponding to the plane σ generated by $\mathbf{e}_{(1)}$ and $\mathbf{e}_{(2)}$ at $\gamma(s)$, and then Eq. (22) can be expressed as

$$\begin{aligned}K(\sigma) = K(\mathbf{e}_{(1)},\mathbf{e}_{(2)}) &= \frac{R_{ljhk}e^l_{(1)}e^h_{(1)}e^j_{(2)}e^k_{(2)}}{(g_{lh}g_{jk} - g_{lk}g_{jh})e^l_{(1)}e^h_{(1)}e^j_{(2)}e^k_{(2)}}\\ &= \frac{1}{|g_{ij}|}R_{1212} = \frac{\hat{R}}{2},\end{aligned} \tag{23}$$

where $K(\sigma)$ is the scalar (Gaussian) curvature. Now Eq. (19) can be written as

$$\begin{aligned}\frac{d^2J^1}{ds^2} &= 0,\\ \frac{d^2J^2}{ds^2} &= -\frac{R_{1212}}{|g_{ij}|}J^2 = -\frac{\hat{R}(s)}{2}J^2.\end{aligned} \tag{24}$$

The evolution of J^1 is linear, and stability is ruled by the scalar J^2 (referred as J) along the reference geodesic, whose evolution with t is given by

$$\frac{d^2J}{dt^2} - \frac{1}{W}\frac{dW}{dt}\frac{dJ}{dt} + 2W^2\hat{R}J = 0, \tag{25}$$

with $2W = 2[E - V(\mathbf{q})] = 2T$ and where the scalar curvature $\hat{R}/2$ determines the local stability around the reference trajectory,

$$\hat{R} = 2\tilde{\mathcal{R}} + \frac{(N-1)}{8W^3}\{4W\nabla^2V + (6-N)|\nabla V|^2\}, \tag{26}$$

with $\tilde{\mathcal{R}}$ the scalar curvature for the metric $a_{ij}(\mathbf{q})$, $|\nabla V|^2 = a^{ij}\partial_iV\partial_jV$, and ∇^2 the Laplacian-Beltrami operator

$$\nabla^2V = a^{ij}\nabla_i\nabla_jV = a^{ij}\left(\frac{\partial^2V}{\partial x^i\partial x^j} - \tilde{\Gamma}^k_{ji}\frac{\partial V}{\partial x^k}\right), \tag{27}$$

where $\tilde{\Gamma}^k_{ji}$ is the Christoffel symbols for $a_{ij}(\mathbf{q})$.

2. The JLC equation for the three-dimensional case

Similarly for the case with $N = 3$ and the comoving basis set, $\{\mathbf{e}_{(1)},\mathbf{e}_{(2)},\mathbf{e}_{(3)}\}$, the Riemann-Christoffel curvature tensor (12) components now read

$$\begin{aligned}&\langle R(\mathbf{e}_{(1)},\mathbf{e}_{(m)})\mathbf{e}_{(1)},\mathbf{e}_{(n)}\rangle = R_{ljhk}\mathbf{e}^l_{(1)}\mathbf{e}^j_{(m)}\mathbf{e}^h_{(1)}\mathbf{e}^k_{(n)}\\ &= R_{1212}\{[\mathbf{e}^1_{(1)}\mathbf{e}^2_{(m)} - \mathbf{e}^2_{(1)}\mathbf{e}^1_{(m)}][\mathbf{e}^1_{(1)}\mathbf{e}^2_{(n)} - \mathbf{e}^2_{(1)}\mathbf{e}^1_{(n)}]\}\\ &\quad + R_{1213}\{[\mathbf{e}^1_{(1)}\mathbf{e}^2_{(m)} - \mathbf{e}^2_{(1)}\mathbf{e}^1_{(m)}][\mathbf{e}^1_{(1)}\mathbf{e}^3_{(n)} - \mathbf{e}^3_{(1)}\mathbf{e}^1_{(n)}]\}\\ &\quad + R_{1213}\{[\mathbf{e}^1_{(1)}\mathbf{e}^2_{(n)} - \mathbf{e}^2_{(1)}\mathbf{e}^1_{(n)}][\mathbf{e}^1_{(1)}\mathbf{e}^3_{(m)} - \mathbf{e}^3_{(1)}\mathbf{e}^1_{(m)}]\}\\ &\quad + R_{1223}\{[\mathbf{e}^1_{(1)}\mathbf{e}^2_{(m)} - \mathbf{e}^2_{(1)}\mathbf{e}^1_{(m)}][\mathbf{e}^2_{(1)}\mathbf{e}^3_{(n)} - \mathbf{e}^3_{(1)}\mathbf{e}^2_{(n)}]\}\\ &\quad + R_{1223}\{[\mathbf{e}^1_{(1)}\mathbf{e}^2_{(n)} - \mathbf{e}^2_{(1)}\mathbf{e}^1_{(n)}][\mathbf{e}^2_{(1)}\mathbf{e}^3_{(m)} - \mathbf{e}^3_{(1)}\mathbf{e}^2_{(m)}]\}\\ &\quad + R_{1313}\{[\mathbf{e}^1_{(1)}\mathbf{e}^2_{(m)} - \mathbf{e}^2_{(1)}\mathbf{e}^1_{(m)}][\mathbf{e}^2_{(1)}\mathbf{e}^3_{(n)} - \mathbf{e}^3_{(1)}\mathbf{e}^2_{(n)}]\}\\ &\quad + R_{1323}\{[\mathbf{e}^1_{(1)}\mathbf{e}^3_{(m)} - \mathbf{e}^3_{(1)}\mathbf{e}^1_{(m)}][\mathbf{e}^1_{(1)}\mathbf{e}^3_{(n)} - \mathbf{e}^3_{(1)}\mathbf{e}^2_{(n)}]\}\\ &\quad + R_{1323}\{[\mathbf{e}^1_{(1)}\mathbf{e}^3_{(n)} - \mathbf{e}^3_{(1)}\mathbf{e}^1_{(n)}][\mathbf{e}^2_{(1)}\mathbf{e}^3_{(m)} - \mathbf{e}^3_{(1)}\mathbf{e}^2_{(m)}]\}\\ &\quad + R_{2323}\{[\mathbf{e}^2_{(1)}\mathbf{e}^3_{(m)} - \mathbf{e}^3_{(1)}\mathbf{e}^2_{(m)}][\mathbf{e}^2_{(1)}\mathbf{e}^3_{(n)} - \mathbf{e}^3_{(1)}\mathbf{e}^2_{(n)}]\},\end{aligned} \tag{28}$$

and taking $\dot{\gamma}(s) = \mathbf{v} = \mathbf{e}_{(1)}$ the JLC equation (13) is

$$\frac{d^2\mathbf{J}}{ds^2} + \mathbb{S}\,\mathbf{J} = 0 \tag{29}$$

with the stability matrix $\mathbb{S}$

$$\mathbb{S} = \begin{bmatrix} 0 & 0 & 0 \\ 0 & \langle R(\mathbf{e}_{(1)}, \mathbf{e}_{(2)})\mathbf{e}_{(1)}, \mathbf{e}_{(2)}\rangle & \langle R(\mathbf{e}_{(1)}, \mathbf{e}_{(3)})\mathbf{e}_{(1)}, \mathbf{e}_{(2)}\rangle \\ 0 & \langle R(\mathbf{e}_{(1)}, \mathbf{e}_{(2)})\mathbf{e}_{(1)}, \mathbf{e}_{(3)}\rangle & \langle R(\mathbf{e}_{(1)}, \mathbf{e}_{(3)})\mathbf{e}_{(1)}, \mathbf{e}_{(3)}\rangle \end{bmatrix}. \tag{30}$$

With the sectional curvatures $\langle R(\mathbf{e}_{(1)}, \mathbf{e}_{(2)})\mathbf{e}_{(1)}, \mathbf{e}_{(2)}\rangle$ and $\langle R(\mathbf{e}_{(1)}, \mathbf{e}_{(3)})\mathbf{e}_{(1)}, \mathbf{e}_{(3)}\rangle$ in the diagonal.

C. Conjugate points and Maslov indices

In this subsection, we consider the points where singularities in the variational principle (7) occur along a reference geodesic, which are known as conjugate or focal points. One interesting consequence of these singularities is that conjugate points tell when geodesics fail to be length minimizing. Actually, all geodesics are locally, but not globally, length minimizing.

Indeed, when the dynamics of the system is integrable, so that motions take place in phase space on the surface of invariant tori [7], the corresponding set of points in configuration space, known as the *caustics* of the system [56], constitutes a sort of limiting set for the trajectories [57]. In the optical or eikonal version, i.e., when light rays are considered, these neighborhoods present interesting accumulations [56] of rays, showing a variety of different characteristics, which are accounted for by catastrophe theory [14,15]. On the other hand, when the dynamics is ergodic, all periodic orbits are unstable and isolated, but nevertheless they constitute an skeleton for the classical chaos, through the associated homoclinic and heteroclinic tangles, as shown by Poincaré [7] and also by Gutzwiller [20] in quantum mechanics. Moreover, these indices are related to the probability density accumulations emerging in the projection over the coordinate space correlating with turning points and caustics located at the conjugate points [16].

Taking into account our purpose in this section, we start with the following definitions:

(1) Let $\gamma : [0, a] \longmapsto M$ be a geodesic line, the point $Q = \gamma(t_1)$ with $t_1 \in (0, a]$ is *conjugate* to another point $P = \gamma(0)$ if there exists a vector field $\mathbf{J}$ along γ fulfilling the JLC equation (13) (Jacobi field) such that $\mathbf{J}(0) = 0 = \mathbf{J}(t_1)$.

(2) The maximum number of such Jacobi fields linearly independent is called the *multiplicity* of the conjugate point $\gamma(t_1)$. Taking into account that $\mathbf{J} = \dot{\gamma}$ is a Jacobi field along γ that never vanishes, so the multiplicity never exceeds $N - 1$.

In order to find the conjugate points along a reference geodesic line, we need to follow the evolution of the modulus $\|\mathbf{J}\|$, with

$$\|\mathbf{J}\|^2 = \langle \mathbf{J}, \mathbf{J}\rangle = g_{ij}J^iJ^j, \tag{31}$$

integrating the JLC equation (13) together with the corresponding Hamilton equations, to find out the points where it cancels.

In this case, instead of using the previously defined parallely transported comoving frame $\{\mathbf{e}_{(1)}, \mathbf{e}_{(2)}\}$, a better alternative is to use the comoving frame $\{\mathbf{e}_T, \mathbf{e}_J\}$, where $\mathbf{e}_T$ is the vector tangent to the geodesic line and $\mathbf{e}_J$ the vector pointing in the direction of $\mathbf{J}$, i.e., $\mathbf{J} = \|\mathbf{J}\|\,\mathbf{e}_J$. Obviously, $D\mathbf{e}_T/ds = 0$ but $D\mathbf{e}_J/ds$ does not necessarily cancel, since its evolution depends on the dynamics, and in general it is not parallelly transported. In any case, when $\|\mathbf{e}_J\| = \|\mathbf{e}_T\| = 1$, the evolution for $\|J\|$ is given by

$$\frac{d^2}{ds^2}\|\mathbf{J}\| = \left[-\langle R(\mathbf{e}_T, \mathbf{e}_J)\mathbf{e}_T, \mathbf{e}_J\rangle + \left\|\frac{D}{ds}\mathbf{e}_J\right\|^2\right]\|\mathbf{J}\|, \tag{32}$$

where $\langle R(\mathbf{e}_T, \mathbf{e}_J)\mathbf{e}_T, \mathbf{e}_J\rangle = \langle R(\mathbf{e}_T, \mathbf{J}/\|\mathbf{J}\|)\mathbf{e}_T, \mathbf{J}/\|\mathbf{J}\|\rangle = K(\mathbf{e}_T, \mathbf{e}_J) = K(s)$ is the sectional curvature at the plane generated by $\mathbf{e}_T$ and $\mathbf{e}_J$. Moreover, in local coordinates

$$\begin{aligned} K(s) &= \left\langle R\left(\mathbf{e}_T, \frac{\mathbf{J}}{\|\mathbf{J}\|}\right)\mathbf{e}_T, \frac{\mathbf{J}}{\|\mathbf{J}\|}\right\rangle \\ &= R_{ijkl}\frac{J^i}{\|\mathbf{J}\|}\frac{dq^j}{ds}\frac{J^k}{\|\mathbf{J}\|}\frac{dq^l}{ds} \end{aligned} \tag{33}$$

and

$$\frac{d^2\|\mathbf{J}\|}{ds^2} = \left(-R_{ijkl}\frac{J^i}{\|\mathbf{J}\|}\frac{dq^j}{ds}\frac{J^k}{\|\mathbf{J}\|}\frac{dq^l}{ds} + \left\|\frac{D}{ds}\mathbf{e}_J\right\|^2\right)\|\mathbf{J}\|. \tag{34}$$

The above referenced integration is repeated for the $N - 1$ linearly independent vectors (recall definition 2) initially at the point $\gamma(0)$, except for the Jacobi field $\mathbf{J} = \dot{\gamma}$.

Considering these vectors as initial conditions for the separation vector $\mathbf{J}(t)$ to integrate the Jacobi equation Eq. (13) or Eq. (34), so that each Jacobi field found with $\mathbf{J}(0) = \mathbf{J}(t_1) = 0$ increases one unit the multiplicity of the conjugate point $\gamma(t_1)$. Notice that there are traversal and longitudinal contributions to the Maslov index determined by the conjugate points and the turning points, respectively.

Calling m_ℓ the multiplicity for the conjugate point ℓ fulfilling $0 \leqslant m_\ell \leqslant N - 1$, we can calculate de Maslov index μ_γ for the periodic orbit $\gamma(t)$ with the expression

$$\mu_\gamma = \sum_\ell m_\ell + P, \tag{35}$$

where P is the total turning points along the orbit during one period. The extra contribution P in (35) needs to be added because of the singularity in the Jacobi equation (13) when the trajectory velocity nullifies, i.e., $\dot{\gamma} = 0$, something that occurs at the turning points and the orbit turns back on itself [see, for example, Figs. 9(a), 9(b), 9(d), and 9(f) below].

III. NUMERICAL RESULTS

A. Two-dimensional quartic oscillator

Let us consider next the use of the geometrodynamic method in the quantization of the two-dimensional coupled quartic oscillator of unit mass

$$H(p_x, p_y, x, y) = \frac{1}{2}\left(p_x^2 + p_y^2\right) + \frac{(1-\alpha)}{12}(x^4 + y^4) + \frac{1}{2}x^2y^2. \tag{36}$$

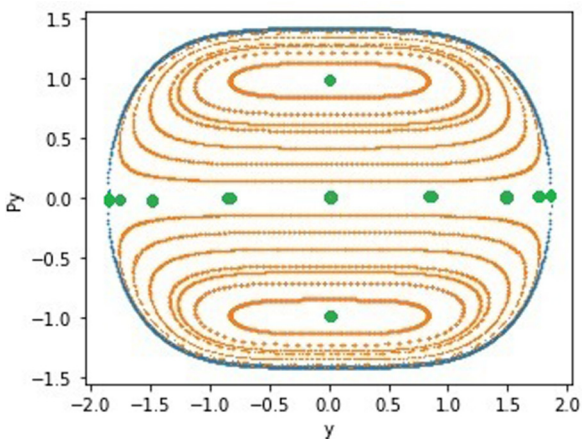

FIG. 3. Composite Poincaré surface of section corresponding to the sectioning surface $(x = 0, p_x > 0)$ at $E = 1$ showing the phase-space structure for the two-dimensional quartic oscillator (36) with $\alpha = 0$. As can be seen, it consists of invariant tori centered around the two fixed points located at $(x = 0, p_x = \pm 1)$ (marked in green) which correspond to the diagonal periodic orbits $y = \pm x$ [see Fig. 4(a)], plus an infinite number of other fixed points on the $p_y = 0$ line, nine of which have been marked in green and correspond to the elliptically shaped periodic orbits shown in Figs. 4(b)–4(e).

We take $\alpha \leqslant 1$, since otherwise the motion is unbounded, as easily ascertain expressing the potential in polar coordinates: $V(r, \theta) = r^4[1 - \alpha + 2(2 + \alpha)\cos^2\theta \sin^2\theta]/12$. The quartic oscillator (36) is known to be highly chaotic for most values of the parameter α and integrable only for $\alpha = -2$ (central potential) and $\alpha = 0$ [58] (as graphically shown in Fig. 3). Moreover, the quartic potential has a high symmetry corresponding to the point group C_{4v}, and very interesting properties derived from fact that they are a homogeneous polynomial in coordinates and momenta. Indeed, for this reason it exhibits mechanical similarity, i.e., trajectories at different values of the energy are related by

$$\begin{aligned} x'(t') &= \eta\, x(t), \quad & p'_x(t') &= \eta^2\, p_x(t) \\ y'(t') &= \eta\, y(t), \quad & p'_y(t') &= \eta^2\, p_y(t), \end{aligned} \tag{37}$$

where time an action are scaled as

$$t' = \eta^{-1} t, \quad \text{with } \eta = \left(\frac{E'}{E}\right)^{1/4}, \tag{38}$$

$$S'(t') = \eta^3 S(t). \tag{39}$$

and then the phase-space structure is invariant with energy. Accordingly, we perform in this section all calculations at $E = 1$ without loss of generality. Also, as mentioned before the quantization for the total action S along a given orbit is equivalent to quantize its length with the Jacobi metric (6), so for different energies the lengths for orbits follow the same relation (39).

With respect to the Jacobi equation (24) with $a_{ij} = \delta_{ij}$ the corresponding curvature, calculated as indicated in (26), is

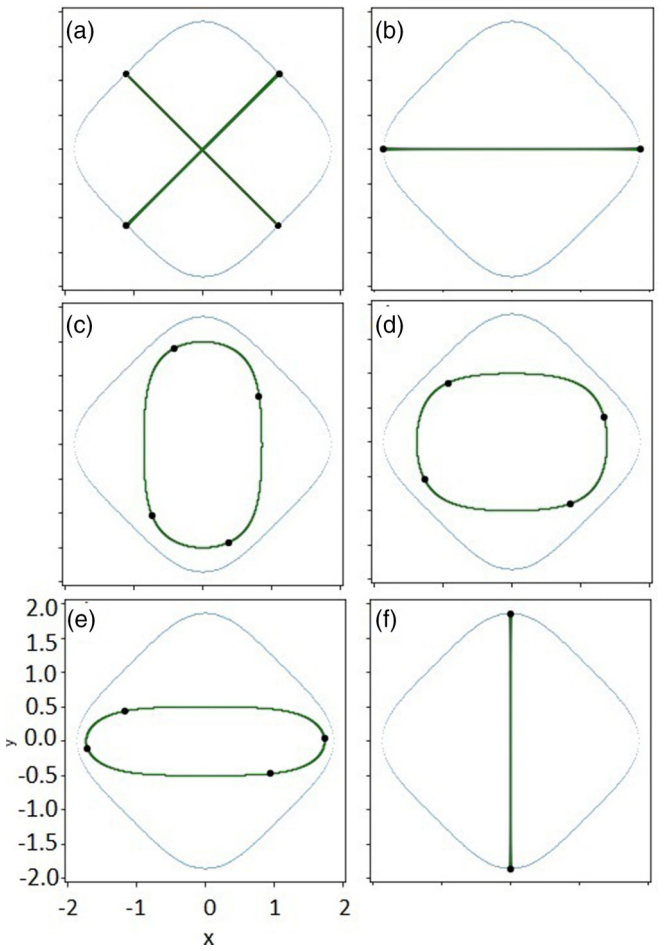

FIG. 4. Trajectories associated to the fixed points marked in green in Fig. 3 corresponding to the $\alpha = 0$ regular case of the coupled quartic oscillator (36). The location of the existing conjugate points are marked with black dots. The isopotential $V = 1$ curve has been added in blue.

given by [59]

$$\hat{R} = \frac{1}{2W^3}\left\{\left[xy^2 + x^3\left(\frac{1-\alpha}{3}\right)\right]^2 + \left[yx^2 + y^3\left(\frac{1-\alpha}{3}\right)\right]^2 + W(2-\alpha)(x^2+y^2)\right\}. \tag{40}$$

1. Integrable case

First, we consider the integrable case corresponding to $\alpha = 0$. In Fig. 3 we present a phase-space view consisting of the (y, p_y) composite Poincaré surface of section (PSOS), taking $(x = 0, p_x > 0)$ as the sectioning surface. As can be seen, it consists of invariant tori, i.e., quasiperiodic trajectories, around the two elliptic fixed points at $(y = 0, p_y = \pm 1)$ which correspond to the diagonal periodic orbits $y = \pm x$ represented in Fig. 4(a). The central horizontal line at $p_y = 0$ is filled with the fixed points of an infinite family of elliptically shaped periodic orbits, five of which are represented in Figs. 4(a)–4(e); they can be traveled either clock $(p_x > 0)$ or anticlockwise $(p_x < 0)$. The corresponding nine (taking into

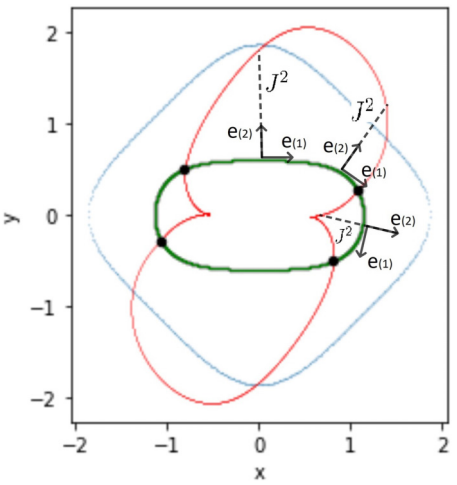

FIG. 5. Evolution of J^2 (red) along one of the elliptically shaped periodic orbit (green) on the $p_y = 0$ line In Fig. 4 showing four conjugate points (black) at the locations where J^2 nullyfies. The comoving frame $\{\mathbf{e}_{(1)}, \mathbf{e}_{(2)}\}$ at three selected points along the trajectory is also shown.

account the $p_x \leftrightarrow -p_x$) fixed points have also been marked in green in Fig. 3. In this case, the length considering the Jacobi metric for all periodic orbits is constant and is equal to 9.2021, as it is also equal to the value of the action S along one period. Superimposed to the orbits we have plotted in black in Fig. 4 the location of the four [two in the case of orbits in Figs. 4(a), 4(b), and 4(f)] corresponding conjugate points that appear when these orbits are traveled clockwise, indicating that $\mu = 4, 2$ in this case.

To analyze in more detail the results concerning the conjugate points, we present in Fig. 5 in red the evolution of the separation vector component J^2 along one of the elliptically shaped periodic orbit on the $p_y = 0$ line In Fig. 4, plotting also superimposed the comoving frame $\{\mathbf{e}_{(1)}, \mathbf{e}_{(2)}\}$ at three selected points of the trajectory. As can be seen, the conjugate points are located at the points of the orbit where the modulus of the vector separation [see Eq. (34)] nullifies. More quantitative details are given in Fig. 6, where a comparison of the values of three relevant physical magnitudes (in logarithmic scale), namely the separation vector (red), the scalar curvature (green), and the kinetic energy (blue), along the orbit as a function of its x coordinate is presented. In it, it is observed that the curvature and the kinetic energy behave inversely, as expected from Eq. (40).

Finally, notice in Fig. 4 how the location of the conjugate points move along the orbits in a continuous fashion as the horizontal (or vertical) periodic orbit is approached. Actually, the associated locus equation in phase space can be analytically calculated, as it is equal to

$$\frac{1}{2}p_x^2 + \frac{1}{12}x^4 = 1, \tag{41}$$

which is homeomorphic to $\mathbb{S}^1$. Accordingly, its projection on the coordinates space is one dimensional with two turning points, implying that the Maslov index is $\mu = P = 2$. This change in the value for the Maslov index results from the change of topology for the orbit in the invariant torus. The

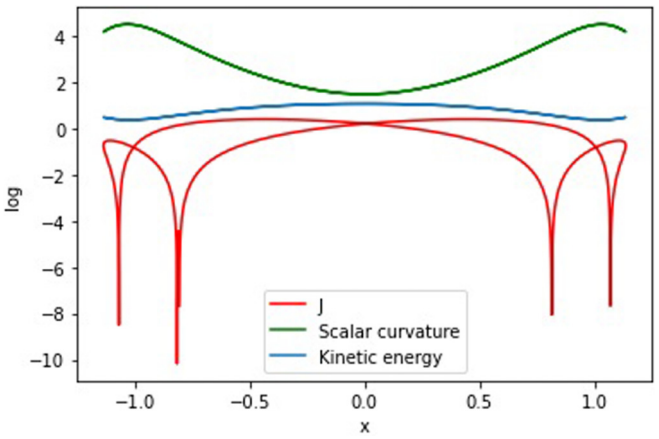

FIG. 6. Evolution of J^2 (red), scalar curvature (green), and kinetic energy (blue) in a decimal logarithmic scale for the trajectory in Fig. 5 as a function of its x coordinate.

same happens for the independent (nonhomotopic) vertical orbit

Let us next consider the case of the quasiperiodic trajectories in order to study the caustics of this problem. For this purpose, we present in Fig. 7(a) a representative quasiperiodic trajectory with initial conditions close to the diagonal orbit, i.e., $(x, p_x, y, p_y)_0 = (0, 0, 1.22, 0.7)$. The associated PSOS is presented in Fig. 7(b). As can be seen in the first panel, the corresponding conjugate points (superimposed in black) form a continuous line in the coordinate space that will give

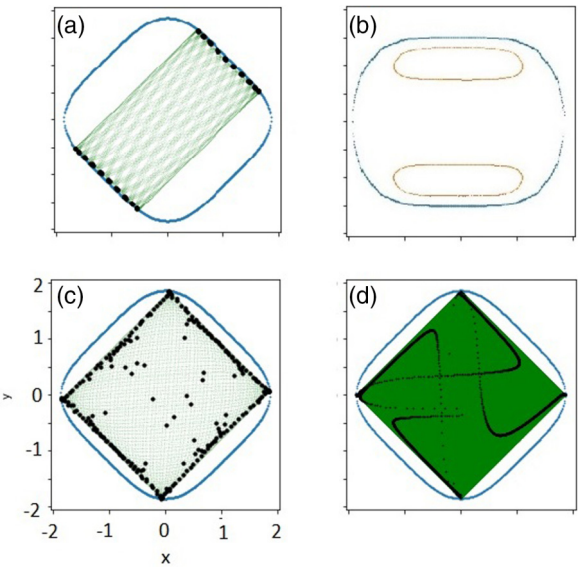

FIG. 7. Caustics and conjugate points for regular quasiperiodic trajectories. (a) Generic quasiperiodic trajectory near the diagonal periodic orbit $y = x$, and (b) associated Poincaré surface of section for the regular coupled quartic oscillator (36) with $\alpha = 0$; the upper-right and lower-left caustic clearly emerge from the computed conjugate points. (c) A similar trajectory with almost equal action in both modes showing the full square caustics; some conjugate points inside the Hill's region are visible. (d) Same as (c) computed with 10 000 trajectories initially launches along the vertical trajectory with $p_x > 0$.

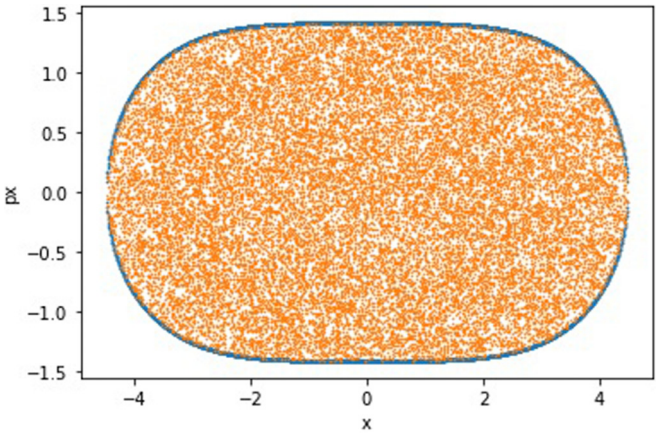

FIG. 8. Same as Fig. 3 for $\alpha = 0.97$ showing the chaotic nature of the corresponding dynamics.

rise to the full caustics if the elapsed time were sufficiently long. In Fig. 7(c) we show such longer picture for a trajectory having similar actions in the x and y motions. In this case the initial condition is close to the horizontal orbit, i.e., (0,0,1.4133,0.05). In it, we can see that the caustics are better defined, reaching the four sides of the square border accessible to the orbit. Actually, for this long dynamics we also see a cloud of points inside the Hill's region, since these

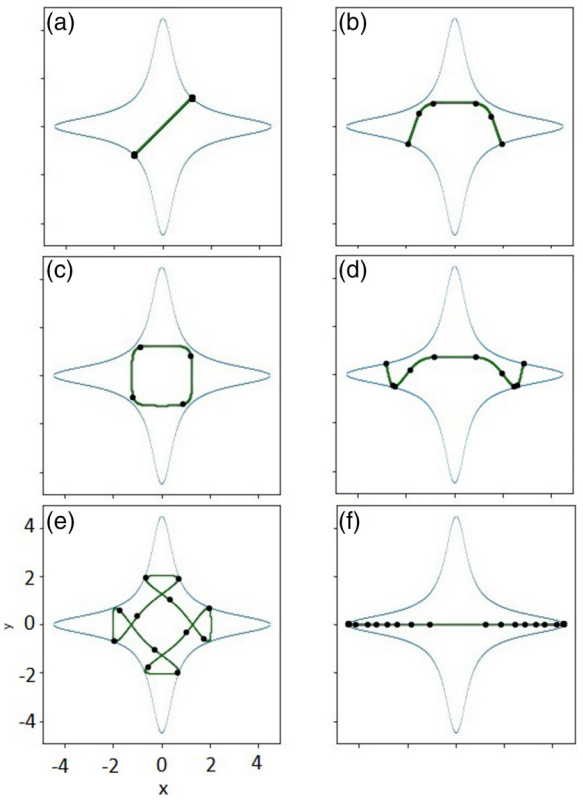

FIG. 9. Selected unstable periodic orbits (green) for $E = 1$ and their Hill's region border $[V(\mathbf{q}) = E]$ (blue) with their conjugate points (black) for quartic oscillator with $\alpha = 0.97$.

TABLE II. Period, action, sum of multiplicities of the conjugate points, number of turning points, and Maslov index for the unstable periodic orbits of Fig. 9. See text for details.

PO	T	S	$\sum_\ell m_\ell$	P	μ
a	6.2216	8.2937	0	2	2
b	10.6899	14.2519	4	2	6
c	7.8432	10.4568	4	0	4
d	14.3738	19.1629	8	2	10
e	7.8432	25.0018	12	0	12
f	16.583	22.1111	14	2	16

mathematical objects usually exhibit a complex geometry. To give an idea of the caustics complexity for this system and the hidden structures that it contains, we also present in Fig. 7(d) the results obtained from 10 000 randomly chosen trajectories with different initial conditions along the vertical y axis and perpendicular to it, i.e., traveling clockwise. The complexity of the curve formed by the conjugate points is very high, and certainly outside the scope of the present work, so we defer its study to a future publication.

However, the important point concerning caustics in relation with this paper is quantization. In this respect, caustics are important, because they can be used to define the torus circuits needed to compute the action appearing in Eq. (1). For this purpose, we could employ, for example, the method described in Ref. [60], and use a quasiperiodic trajectory that almost return to the initial point in phase space after N_x periods in the x coordinate and N_y in y, thus obtaining

$$S(E_{n_x,n_y}) = 2\pi(N_x n_x + N_y n_y) + \pi(N_x + N_y), \tag{42}$$

where n_x and n_y are the corresponding quantum numbers and taking into account that, in this case, $\mu_x = \mu_y = 1/2$.

2. *Chaotic case*

Let us consider now the chaotic case corresponding to $\alpha = 0.97$. As can be seen in the corresponding PSOS, shown in Fig. 8, the dynamics is highly chaotic [61] and most periodic

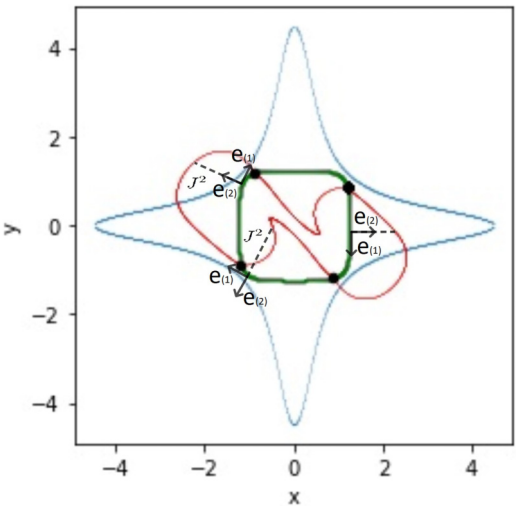

FIG. 10. Same as Fig. 5 for the unstable periodic orbit in Fig. 9(c).

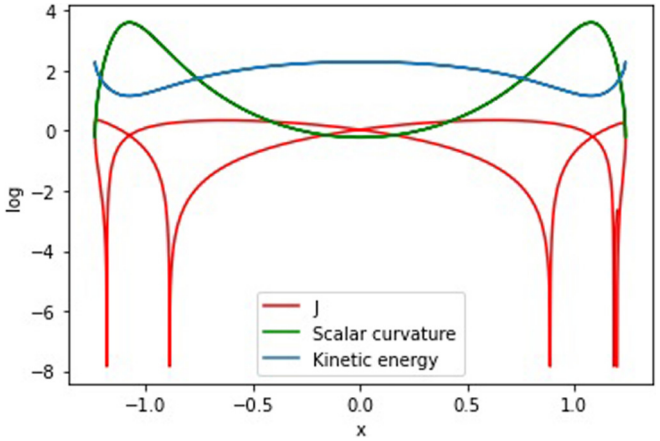

FIG. 11. Same as Fig. 6 for the unstable periodic orbit in Fig. 10(c).

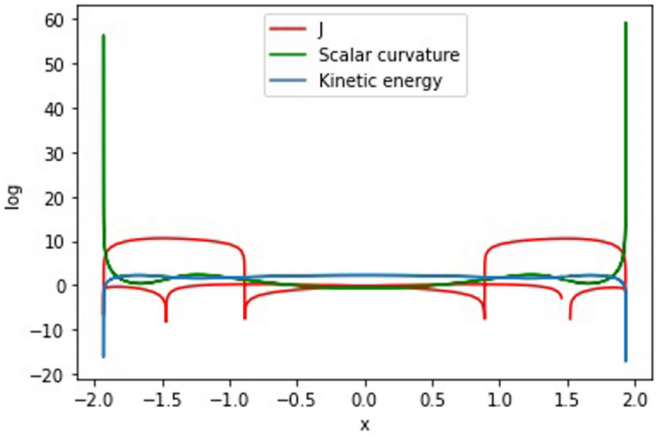

FIG. 13. Same as Fig. 6 for the unstable periodic orbit in Fig. 12(b).

orbits are unstable and isolated [58]. Accordingly, we have selected six of them among the most representative [17], which are shown in Fig. 9. The corresponding conjugate points have been represented superimposed, and their principal dynamical characteristics in connection to quantization, for example to calculate scarred functions [17], have been summarized in Table II. As can be seen the number of conjugate points varies from just two at the turning points for the diagonal orbit, to 16 for the apparently simple horizontal one.

To study in more detail the location of the conjugate points we present in Fig. 9 six unstable periodic orbits with their conjugate points. Specially interesting are the self-retracing ones in Figs. 9(a), 9(b), 9(d), and 9(f), causing two turning points to appear at the Hill's border with the contribution of $P = 2$ in expression (35). In Figs. 10 and 12 the evolution for the separation vector component J^2 along two of them is presented, where the comoving frame $\{\mathbf{e}_{(1)}, \mathbf{e}_{(2)}\}$ at different points along the trajectory has also been included. Also, in Figs. 11 and 13, we compare three relevant magnitudes, namely the separation vector, the scalar curvature, and the kinetic energy as a function of the x coordinate of the position

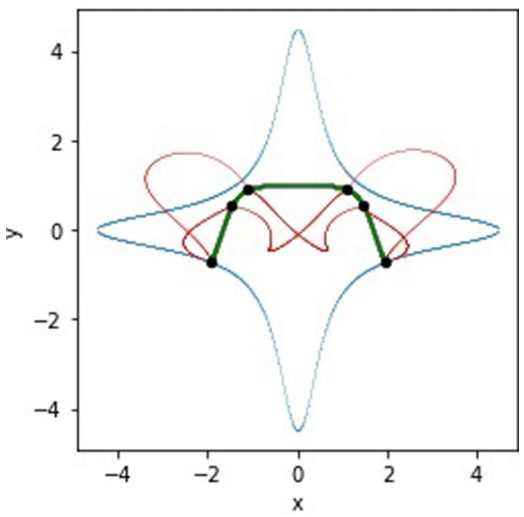

FIG. 12. Same as Fig. 5 for the unstable periodic orbit in Fig. 9(b).

along the orbit presented in Figs. 10 and 12 measured in a logarithmic scale.

B. Hydrogen atom

To conclude this section, we discuss the application of the geometrodynamic method to the hydrogen atom, a three-dimensional problem that as discussed in the Introduction played an important role in the development of the quantum theory [1]. The corresponding dynamics is separable with a central Coulomb potential,

$$V(r) = -\frac{e^2}{r}. \tag{43}$$

In the phase space the Hamiltonian in spherical coordinates (r, ϕ, θ) reads

$$H(r, \phi, \theta, p_r, p_\phi, p_\theta) = \frac{1}{2m_e}\left(p_r^2 + \frac{1}{r^2}p_\phi^2 + \frac{1}{r^2 \sin^2\phi}p_\theta^2\right) - \frac{e^2}{r}. \tag{44}$$

The Jacobi metric expression (6) for the MM is then

$$g_{ij}(r, \phi, \theta) = 2m_e\left(E + \frac{e^2}{r}\right)\begin{pmatrix} 1 & 0 & 0 \\ 0 & r^2 & 0 \\ 0 & 0 & r^2 \sin^2\phi \end{pmatrix}. \tag{45}$$

The non-null Christoffel symbols are

$$\begin{aligned}
\Gamma^r_{rr} &= -\frac{e^2}{2r(Er + e^2)}, \\
\Gamma^r_{\phi\phi} &= -\frac{r(2Er + e^2)}{2(Er + e^2)} = \frac{\Gamma^r_{\theta\theta}}{\sin^2\phi}, \\
\Gamma^\phi_{r\phi} &= \frac{Er + (e^2/2)}{r(Er + e^2)} = \Gamma^\phi_{\phi r} = \Gamma^\theta_{r\theta} = \Gamma^\theta_{\theta r}, \\
\Gamma^\phi_{\theta\theta} &= -\tfrac{1}{2}\sin(2\phi), \\
\Gamma^\theta_{\phi\theta} &= \frac{1}{\tan\phi} = \Gamma^\theta_{\theta\phi},
\end{aligned} \tag{46}$$

and the geodesic lines fulfill

$$\frac{d^2r}{ds^2} - \frac{e^2}{2r(Er+e^2)}\left(\frac{dr}{ds}\right)^2 - \frac{r(2Er+e^2)}{2(Er+e^2)}\left[\left(\frac{d\phi}{ds}\right)^2 + \sin^2\phi\left(\frac{d\theta}{ds}\right)^2\right] = 0,$$
$$\frac{d^2\phi}{ds^2} + 2\frac{Er+\frac{e^2}{2}}{r(Er+e^2)}\frac{dr}{ds}\frac{d\phi}{ds} - \frac{1}{2}\sin(2\phi)\left(\frac{d\theta}{ds}\right)^2 = 0,$$
$$\frac{d^2\theta}{ds^2} + 2\frac{Er+\frac{e^2}{2}}{r(Er+e^2)}\frac{dr}{ds}\frac{d\theta}{ds} + \frac{2}{\tan\phi}\frac{d\phi}{ds}\frac{d\theta}{ds} = 0. \tag{47}$$

As deduced from the geodesic equations (47) any geodesic line corresponding to the circular orbit γ fulfills the condition $E = V/2 = -e^2/(2r)$ (virial theorem) with $E < 0$, or $r = -e^2/(2E)$, that in polar coordinates read

$$\begin{aligned} r(t) &= r, \\ \phi(t) &= t, \quad 0 \leqslant t \leqslant 2\pi, \\ \theta(t) &= \theta_0, \quad \theta_0 \in (0, 2\pi], \end{aligned} \tag{48}$$

We consider the comoving basis $\{\mathbf{e}_{(1)}, \mathbf{e}_{(2)}, \mathbf{e}_{(3)}\}$

$$\begin{aligned} \mathbf{e}_{(1)} &= \lambda_1\mathbf{e}_\phi = \frac{1}{\sqrt{e^2m_er}}\mathbf{e}_\phi \\ \mathbf{e}_{(2)} &= \lambda_2\mathbf{e}_r = \frac{r}{\sqrt{e^2m_er}}\mathbf{e}_r \\ \mathbf{e}_{(3)} &= \frac{\lambda_3}{\sin\phi}\mathbf{e}_\theta = \frac{1}{\sin\phi\sqrt{e^2m_er}}\mathbf{e}_\theta, \end{aligned} \tag{49}$$

and the sectional curvatures appearing in the stability matrix (30) for the JLC equation (29),

$$\begin{aligned} K(\mathbf{e}_{(1)}, \mathbf{e}_{(2)}) &= \frac{R_{1212}}{g_{22}g_{11} - g_{12}^2} = \frac{1}{e^2m_er} \\ K(\mathbf{e}_{(1)}, \mathbf{e}_{(3)}) &= \frac{R_{2323}}{g_{22}g_{33} - g_{23}^2} = \frac{1}{e^2m_er}. \end{aligned} \tag{50}$$

Therefore the form for the JLC equations (29) as a function of the parameter t is

$$\begin{aligned} \frac{d^2J^1}{dt^2} &= 0 \\ \frac{d^2J^2}{dt^2} &= -\frac{e^2}{m_er^3}J^2 \\ \frac{d^2J^3}{dt^2} &= -\frac{e^2}{m_er^3}J^3, \end{aligned} \tag{51}$$

with both sectional curvatures equal to $K = e^2/(m_er^3)$, that for the circular orbit $r = -e^2/(2E)$ reads $K = -8E^3/e^4$. Accordingly, the Jacobi fields are

$$\mathbf{J}^i(t) = \frac{\sin(\sqrt{K}t)}{\sqrt{K}}\mathbf{w}(t), \qquad i = 1, 2, \tag{52}$$

where $\mathbf{w}(t)$ is the parallel field along the trajectory, with $\mathbf{J}^i(0) = \mathbf{J}^i(\pi\sqrt{m_er^3}/e) = 0$, so that the antipodal point $\gamma(\pi\sqrt{m_er^3}/e)$ is a conjugate point for $\gamma(0)$. The circular orbits considered by Bohr for the hydrogen atom have no turning points, and there exist two different linearly independent Jacobi fields, therefore the multiplicity is 2, and Eq. (35) for Maslov index for these circular orbit asserts that

$$\mu(E) = \sum_\ell m_\ell + P = 2 + 2 + 0 = 4. \tag{53}$$

Considering the EBK quantization condition for the circular trajectories $\gamma(t) = (-e^2/(2E), t, \theta_0)$ with $t \in (0, 2\pi]$, then $\dot\gamma(t) = (0, 1, 0)$, we can calculate the length L with the Jacobi metric (45)

$$\|\dot\gamma\|^2 = -2m_eE(0 \quad 1 \quad 0)\begin{pmatrix} 1 & 0 & 0 \\ 0 & \frac{e^4}{4E^2} & 0 \\ 0 & 0 & \frac{e^4}{4E^2}\sin^2 t \end{pmatrix}\begin{pmatrix} 0 \\ 1 \\ 0 \end{pmatrix} \tag{54}$$

and then

$$\|\dot\gamma\| = \sqrt{-\frac{e^4m_e}{2E}}, \tag{55}$$
$$L = \oint \|\dot\gamma(t)\|dt = \oint \sqrt{-\frac{e^4m_e}{2E}}dt = 2\pi\sqrt{-\frac{e^4m_e}{2E}}. \tag{56}$$

As the action S along the orbit during a period coincides with its length in the MM, i.e., measured with Jacobi metric, the quantization condition (1) with $\mu = 4$ gives

$$\sqrt{-\frac{e^4m_e}{2E}}2\pi = 2\pi\hbar(n+1), \quad n = 0, 1, 2, \ldots, \tag{57}$$

and the quantized energies are

$$E_n = \frac{-e^4m_e}{2(n+1)^2\hbar^2}, \quad n = 0, 1, 2, \ldots, \tag{58}$$

where the ground-state energy

$$E_0 = \frac{-e^4m_e}{2\hbar^2} \tag{59}$$

and the orbit radius is

$$r_n = \frac{(n+1)^2\hbar^2}{e^2 m_e} = (n+1)^2 a_0, \tag{60}$$

where $r_0 = a_0 = \dfrac{\hbar^2}{e^2 m_e}$ the Bohr radius.

IV. CONCLUSIONS AND DISCUSSION

In this work we have presented an original geometrical method to compute the location of conjugate points of classical trajectories and calculate Maslov indices for periodic orbits in conservative dynamical systems with quadratic (in momenta) kinetic functions. We have showed that the method, based on the classical Jacobi equation in the geometrodynamic formalism, is coordinate independent and can easy transferred among different systems and, moreover, generalized to any dimensionality. As an illustration, we have applied the method for the two-dimensional coupled quartic oscillator system, in both the integrable and chaotic regimes, and also to the three-dimensional circular hydrogen atom, showing the method gives correct results in all cases.

We emphasize the important role of the geometrodynamic formalism as an invariant and fruitful way to investigate dynamical system. Actually, the present paper represents, in some sense, a continuation of our previous work, in which we defined new descriptors for the chaotic behavior in molecular reactive systems using the same method.

ACKNOWLEDGMENTS

This work has been partially supported by the Spanish Ministry of Science, Innovation and Universities, Gobierno de España, under Contracts No. PGC2018-093854-BI00 and ICMAT Severo Ochoa No. CEX2019-000904-S, and by the People Program (Marie Curie Actions) of the European Union's Horizon 2020 Research and Innovation Program (Grant No. 734557). A.V. and J.M. gratefully acknowledge support from Margarita Salas Contract No. UP2021-035 financed by the European Union-NextGenerationEU.

[1] N. Bohr, On the constitution of atoms and molecules, Part I, Phil. Mag. **26**, 1 (1913).
[2] A. Sommerfeld, Zur Quantentheorie der spektrallinien, Ann. Phys. (Berl.) **50**, 489 (1916).
[3] P. S. Epstein, Zur theorie des Starkeffectes, Ann. Phys. (Berl.) **51**, 1 (1916).
[4] A. Einstein, Beitrage zur quantentheorie, Dtsch. Phys. Ges. Verh. **16**, 826 (1914).
[5] P. Ehrenfest, Adiabatic invariants and the theory of quanta, Phil. Mag. **33**, 500 (1917).
[6] A. Einstein, Dtsch. Phys. Ges. Verh. **19**, 82 (1917).
[7] A. J. Lichtenberg and M. A. Lieberman, *Regular and Chaotic Dynamics* (Springer, New York, 2010).
[8] V. P. Maslov and Feodoriuk, *Semi-Classical Approximation in Quantum Mechanics* (Reidel, Boston, 1981).
[9] L. Brillouin, Remarques sur la mécanique ondulatoire, J. Phys. Radium **7**, 353 (1926).
[10] J. B. Keller, Corrected Bohr-Sommerfeld quantum conditions for nonseparable systems, Ann. Phys. **4**, 180 (1958).
[11] R. H. Dicke and J. P. Wittke, *Introduction to Quantum Mechanics* (Addison-Wesley, Reading, MA, 1960).
[12] A. Lahiri, *Basic Optics: Principles and Concepts* (Elsevier, Amsterdam, 2016).
[13] H. A. Buchdahl, *An Introduction to Hamiltonian Optics* (Cambridge University Press, Cambridge, UK, 1970).
[14] T. Poston and J. Stewart, *Catastrophe Theory and Its Applications* (Pitman, London, 1978).
[15] V. I. Arnold, *Catastrophe Theory* (Springer-Verlag, Berlin, 1986).
[16] E. J. Heller, *The Semiclassical Way to Dynamics and Spectroscopy* (Princeton University Press, Princeton, NJ, 2018).
[17] F. Revuelta, E. G. Vergini, R. M. Benito, and F. Borondo, Computationally efficient method to construct scar functions, Phys. Rev. E **85**, 026214 (2012).
[18] F. Revuelta, E. G. Vergini, R. M. Benito, and F. Borondo, Scar functions, barriers for chemical reactivity, and vibrational basis sets, J. Phys. Chem. A **120**, 4928 (2016).
[19] F. Haake, *Quantum Signatures of Chaos*, Springer Series in Synergetics Vol. 54 (Springer, Berlin, 2010).
[20] M. C. Gutzwiller, *Chaos in Classical and Quantum Mechanics* (Springer-Verlag, Berlin, 1991).
[21] M. A. Nielsen and I. L. Chuang, *Quantum Computation and Quantum Information* (Cambridge University Press, India, New Delhi, 2013).
[22] B. Eckhardt and D. Wintgen, Indices in classical mechanics, J. Phys. A: Math. Gen. **24**, 4335 (1991).
[23] L. Bonnet and C. Crespos, Phase-index problem in the semiclassical description of molecular collisions, Phys. Rev. A **78**, 062713 (2008).
[24] M. Beck and S. J. A. Maalham, Computing the Maslov index for large systems, Proc. Am. Math. Soc. **143**, 2159 (2015).
[25] M. P. Carmo, *Differential Geometry of Curves and Surfaces* (Prentice Hall, Englewood Cliffs, NJ, 1976).
[26] M. P. do Carmo, *Riemannian Geometry* (Birkhauser, Boston, 1992).
[27] M. A. Javaloyes and P. Piccione, Comparison results for conjugate and focal points in semi-Riemannian geometry via Maslov indices, Pac. J. Math. **243**, 43 (2009).
[28] V. L. Barutello, D. Offin, A. Portaluri, and L. Wu, Sturm theory with applications in geometry and classical mechanics, Math. Z. **299**, 257 (2021).
[29] L. P. Eisenhart, Dynamical trajectories and geodesics, Ann. Math. **30**, 591 (1928).
[30] M. Di Bari and P. Cipriani, Geometry and chaos on Riemann and Finsler manifolds, Planet. Space Sci. **46**, 1543 (1998).
[31] P. Cipriani and M. Bari, Finsler Geometric Local Indicator of Chaos for Single Orbits in the Henon-Heiles Hamiltonian, Phys. Rev. Lett. **81**, 5532 (1998).
[32] P. Cipriani and M. Bari, Geometry and chaos on Riemann and Finsler manifolds, Planet. Space Sci. **46**, 1499 (1998).
[33] M. Di Bari, D. Boccaletti, P. Cipriani, and G. Pucacco, Dynamical behavior of Lagrangian systems on Finsler manifolds, Phys. Rev. E **55**, 6448 (1997).

[34] L. Di Cairano, M. Gori, and M. Pettini, Coherent Riemannian-geometric description of Hamiltonian order and chaos with Jacobi metric, Chaos **29**, 123134 (2019).
[35] Y. Ben Zion and L. Horwitz, Detecting order and chaos in three-dimensional Hamiltonian systems by geometrical methods, Phys. Rev. E **76**, 046220 (2007); Controlling effect of geometrically defined local structural changes on chaotic Hamiltonian systems, **81**, 046217 (2010).
[36] Y. Ben Zion and L. Horwitz, Applications of geometrical criteria for transition to Hamiltonian chaos, Phys. Rev. E **78**, 036209 (2008).
[37] L. Casetti, R. Livi, and M. Pettini, Gaussian Model for Chaotic Instability of Hamiltonian Flows, Phys. Rev. Lett. **74**, 375 (1995).
[38] L. Casetti, C. Clementi, and M. Pettini, Riemannian theory of Hamiltonian chaos and Lyapunov exponents, Phys. Rev. E **54**, 5969 (1996).
[39] L. Casetti, M. Pettini, and E. G. D. Cohen, Geometric approach to Hamiltonian dynamics and statistical mechanics, Phys. Rep. **337**, 237 (2000).
[40] M. Cerruti-Sola and M. Pettini, Geometric description of chaos in self-gravitating systems, Phys. Rev. E **51**, 53 (1995).
[41] M. Cerruti-Sola and M. Pettini, Geometric description of chaos in two-degrees-of-freedom Hamiltonian systems, Phys. Rev. E **53**, 179 (1996).
[42] C. Clementi and M. Pettini, A geometric interpretation of integrable motions, Celest. Mech. Dyn. Astron. **84**, 263 (2002).
[43] A. Saa, On the viability of local criteria for chaos, Ann. Phys. **314**, 508 (2004).
[44] F. J. Arranz, F. Borondo, and R. M. Benito, Transition from order to chaos in a floppy molecule: LiNC/LiCN, Chem. Phys. Lett. **317**, 451 (2000).
[45] J. C. Losada, J. M. Estebaranz, R. M. Benito, and F. Borondo, Local frequency analysis and the structure of classical phase space of the LiNC/LiCN molecular system, J. Chem. Phys. **108**, 63 (1998).
[46] R. M. Benito, F. Borondo, J.-H. Kim, B. G. Sumpter, and G. S. Ezra, Comparison of classical and quantum phase space structure of nonrigid molecules LiCN, Chem. Phys. Lett. **161**, 60 (1989).
[47] F. Borondo, A. A. Zembekov, and R. M. Benito, Quantum manifestations of saddle-node bifurcations, Chem. Phys. Lett. **246**, 421 (1995).
[48] F. Borondo, A. A. Zembekov, and R. M. Benito, Saddle-node bifurcations in the LiNC/LiCN molecular system: Classical aspects and quantum manifestations, J. Chem. Phys. **105**, 5068 (1996).
[49] A. A. Zembekov, F. Borondo, and R. M. Benito, Semiclassical quantization of fragmented tori: Application to saddle-node states of LiNC/LiCN, J. Chem. Phys. **107**, 7934 (1997).
[50] D. A. Wisniacki, M. Saraceno, F. J. Arranz, R. M. Benito, and F. Borondo, Poincaré-Birkhoff theorem in quantum mechanics, Phys. Rev. E **84**, 026206 (2011).
[51] F. J. Arranz, L. Seidel, C. G. Giralda, R. M. Benito, and F. Borondo, Onset of quantum chaos in molecular systems and the zeros of the Husimi function, Phys. Rev. E **87**, 062901 (2013).
[52] A. Vergel, R. M. Benito, J. C. Losada, and F. Borondo, Geometrical analysis of the LICN vibrational dynamics: A stability geometrical indicator, Phys. Rev. E **89**, 022901 (2014).
[53] A. Vergel, J. C. Losada, R. M. Benito, and F. Borondo, Geometrodynamical analysis to characterize the dynamics and stability of a molecular system through the boundary of the Hill's region, Appl. Math. **5**, 2630 (2014).
[54] K. Ramasubramanian and M. S. Sriram, Global geometric indicator of chaos and Lyapunov exponent in Hamiltonian systems, Phys. Rev. E **64**, 046207 (2001).
[55] L. De Broglie, Recherches sur la théorie des quanta, Ann. Phys. **10**, 22 (1925).
[56] M. V. Berry and C. Upstill, IV catastrophe optics: Morphology of caustics and their diffraction patterns, Prog. Opt. **18**, 257 (1980).
[57] D. W. Noid and R. A. Marcus, Semiclassical calculation of bound states in a multidimensional system. Use of Poincaré's surface of section, J. Chem. Phys. **62**, 2119 (1975).
[58] T. Kapela and C. Simó, Rigorous KAM results around arbitrary periodic orbits for Hamiltonian systems, Nonlinearity **30**, 965 (2017).
[59] N. Caranicolas and C. Sabir, Chaos in a quartic dynamical model, Celest. Mech. **40**, 35 (1987).
[60] W. Eastes and R. A. Marcus, Semiclassical calculation of bound states in a multidimensional system, J. Chem. Phys. **61**, 4301 (1974).
[61] M. P. Joy and M. Sabir, Chaos and curvature in a quartic Hamiltonian system, Pramana J. Phys. **40**, 17 (1993).